

rophages on ice in a stainless steel homogenizer into 20 mM Hepes, 0.5 mM EGTA, 250 mM sucrose, and 0.5% gelatin (pH 7.0) with 10  $\mu$ M TLCK and leupeptin. Unbroken cells and nuclei were sedimented by centrifugation and the supernatant passed through a 3- $\mu$ m pore Nucleopore filter. The flow-through was centrifuged through a 12% sucrose cushion at 1700g for 45 min and collected at the tube base. *Leishmania* phagosomes were isolated into the same lysis mixture by disruption with ~30 passages through 50 mm of 0.6-mm bore plastic tubing. After a low-speed spin to sediment large debris, the supernatant was loaded onto a discontinuous sucrose step gradient (60%, 40%, 20%, and homogenate) and centrifuged at 1700g for 25 min. The phagosomes were harvested from the 40 to 60% interface. The purity of these and subsequent phagosome prep-

arations was monitored by electron microscopy.

17. J. Heuser, Q. Zhu, M. Clarke, *J. Cell Biol.* **121**, 1311 (1993).
18. R. D. Nelson *et al.*, *Proc. Natl. Acad. Sci. U.S.A.* **89**, 3541 (1992).
19. N. Nelson, *Curr. Opin. Cell Biol.* **4**, 654 (1992).
20. M. S. Perin, V. A. Fried, D. K. Stone, X. S. Xie, T. C. Suedhof, *J. Biol. Chem.* **266**, 3877 (1991).
21. I. Mellman, *J. Exp. Biol.* **172**, 39 (1992).
22. N. Marquez-Sterling *et al.*, *Eur. J. Cell Biol.* **56**, 19 (1991).
23. J. Chan *et al.*, *Infect. Immun.* **59**, 1755 (1991).
24. R. Appleberg and I. M. Orme, *Immunology* **80**, 352 (1993).
25. The IgG-beads were prepared by reaction of tosylactivated, iron-containing, 2.8- $\mu$ m latex beads (Dynal) with human IgG. The IgG-bead phagosomes were isolated by lysis of macro-

phages in homogenization buffer by passage through narrow-gauge tubing (16) and washed (four times) after magnetic selection in a Dynal MPC apparatus. SDS-PAGE gels were run with phagosome preparations normalized to equivalent amounts of LAMP-1 protein. Nitrocellulose blots were probed with primary antibodies and species-specific, horseradish peroxidase-conjugated secondary antibodies (Jackson ImmunoResearch Laboratories). The blots were developed by enhanced chemiluminescence (Amersham).

26. Supported by USPHS grants AI26889 and AI34207 (to D.G.R.) and by USPHS award AR42370 (to P.H.S.). D.G.R. would like to thank N. Connell, B. Bloom, I. Orme, and P. Brennan for their introduction to *Mycobacterium*.

23 June 1993; accepted 18 November 1993

## Magnetic Resonance Microscopy of Embryonic Cell Lineages and Movements

Russell E. Jacobs\* and Scott E. Fraser

Key events in vertebrate embryogenesis are difficult to observe in many species. High-resolution magnetic resonance imaging was used to follow cell movements and lineages in developing frog embryos. A single cell was injected at the 16-cell stage with a contrast agent, based on the gadolinium chelate gadolinium-diethylenetriamine pentaacetic acid-dextran. The labeled progeny cells could be followed uniquely in three-dimensional magnetic resonance images, acquired from the embryo over several days. The results show that external ectodermal and internal mesodermal tissues extend at different rates during amphibian gastrulation and neurulation.

The analysis of cell lineages and cell movements is central to an understanding of the processes by which an adult vertebrate develops. The opacity and large number of indistinguishable cells in the vertebrate embryo prohibit analysis by direct observation (1). The tracing of cell movements and lineages requires some means to render a cell and its progeny unique. Individual precursors cells have been labeled with membrane-impermeable enzymes (2) or fluorescent dyes (3), or infected with a retroviral agent (4). With few exceptions (5), subsequent observation of the progeny requires fixed, sectioned, and stained specimens. This processing prohibits the direct observation of ongoing developmental events; instead, they must be inferred by comparison of results obtained from different embryos fixed at different stages.

This limitation is especially critical in studies of early morphogenetic events in the vertebrate embryo, such as gastrulation in amphibians. Although *Xenopus laevis* has served as the central system for analyses of vertebrate gastrulation movements and the cell interactions that they bring about, most of the movements of cells cannot be followed in the intact embryo because they take place largely

within its interior. Thus, analyses of these processes in *X. laevis* have relied on time-lapse cinematography of surface cell movements, histological examination of fixed specimens, and explantation techniques (6). The results of these studies have demonstrated the coupling of the convergence of cells toward the dorsal midline with the extension of the embryonic axis (convergent extension) brought about by changes in cell shape and relative positioning (radial and mediolateral intercalation). Short-range intercalary movements can bring about large-scale tissue movements. For example, a simple mediolateral intercalation of each cell moving between its neighbors toward the midline results in a doubling of the tissue length (extension) and halving of the tissue width (convergence). Explant cultures show such convergence-extension movements during gastrulation, both in the cells that remain on the surface of the embryo (noninvoluting marginal zone) and in those that involute to form the expanding archenteron (involuting marginal zone).

To observe ongoing developmental events in living frog embryos, we used high-resolution magnetic resonance imaging (MRI). With MRI, three-dimensional (3D) images of the developing embryo may be obtained on a time scale faster than the cell division time and analyzed forward or backward in time to reconstruct fully cell divisions and cell movements. The MRI

technique is a qualitatively different method of visualization than the light microscopy used in previous lineage studies. In this method, the recorded signal arises from the hydrogen nuclear spin of water molecules. Spatial localization of the nuclear magnetic resonance (NMR) signal is made possible by superimposing various magnetic field gradients on the usual static magnetic field (7). The use of a set of three orthogonal gradients allows the NMR signal to be parsed into a matrix of intensities, one for each volume element (voxel), yielding the 3D magnetic resonance image. Contrast in the magnetic resonance image arises from voxel-to-voxel variations in the water concentration and local environment. Variations in the local environment (for example, proximity to a paramagnetic center) and state (for example, mobile versus immobile) of the water modulate the NMR relaxation times  $T_1$  and  $T_2$  (8). We use an imaging protocol that yields an image in which the intensity is a monotonic function of the relaxation rate ( $1/T_1$ ) (9).

To perform cell lineage analyses with MRI, an MRI lineage tracer is required that must (i) induce a local signal that is characteristically different from that of the rest of the sample, (ii) be physiologically inert, and (iii) remain within the originally labeled cell and its progeny. MRI contrast enhancement agents based on gadolinium have the needed effect on the MRI water signal, increasing the relaxation rates of nearby nuclear spins to provide contrast not naturally found in the specimen (10). We used an MRI contrast agent that is a covalent conjugate of dextran with diethylenetriamine pentaacetic acid (DTPA) to which  $Gd^{3+}$  has been chelated (11). The high-affinity chelator DTPA protects living systems from the toxic effects of  $Gd^{3+}$  (12). We used twice as much chelator as  $Gd^{3+}$  to ensure that a minimal amount of free  $Gd^{3+}$  was present. The dextran is membrane-impermeant and too large to pass from cell to cell through gap junctions, thereby limiting the contrast agent to the injected cells and their descendants. Because this tracer is

Division of Biology, Beckman Institute (139-74), California Institute of Technology, Pasadena, CA 91125.

\*To whom correspondence should be addressed.

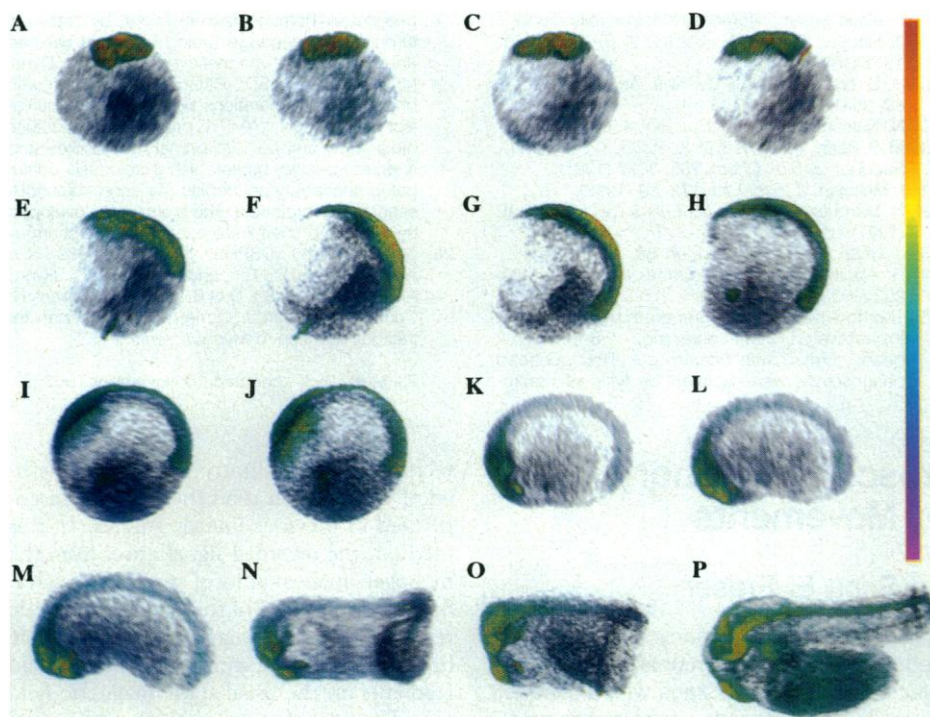
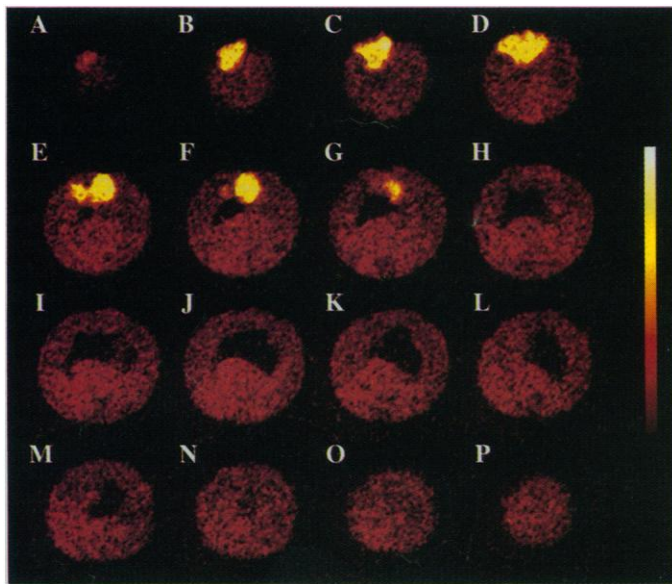


**Fig. 1.** Magnetic resonance images of a single developing frog embryo taken at 16 successive times; (A) to (P) were recorded at 4, 7, 9, 12, 21, 24, 27, 29, 33, 35, 45, 47, 51, 59, 69, and 98 hours after fertilization, respectively. Descendants of a single 16-cell blastomere, injected with the contrast agent (24) 2 hours before the first image was recorded, appear as high-intensity volumes (yellow-red). In (A) to (D), the embryo develops into a blastula. The blastocoel is a lighter gray region to the upper left and the mass of yolk cells are the blue-gray region to the lower right in (D). In (E) to (J), the embryo is undergoing gastrulation. It passes from an early neurula to the early tail bud stage in (K) to (P). For visualization, we used VoxelView (Vital Images, Fairfield, Iowa). In all the figures, the bottom of the color scale bar indicates low intensity and the top high intensity. To permit the labeled cells to be visualized among the unlabeled cells, the opacity of each voxel was adjusted so that higher voxel intensity values have exponentially higher opacity values. Thus cavities are rendered transparent, the unlabeled cells semitransparent, and labeled cells opaque. This display routine is sufficient to display the majority of the labeled cells except for panels (K) to (O), in which the thickness of the somite tissue obscures the display of the labeled clone in the neural tube. The width of the color scale bar represents 125  $\mu\text{m}$ .

**Fig. 2.** (A to P) Sixteen slices through the early blastula stage. The slices are 75  $\mu\text{m}$  apart and 12  $\mu\text{m}$  thick. Each is oriented with the animal pole to the upper left and the future dorsal axis to the right. An intense region near the animal pole is sharply demarcated from its surroundings in this 128-cell embryo. The intense region occupies the volume expected of the eight descendants of the originally labeled cell. Within the high-intensity region, the several small low-intensity regions (D) are the nuclei of the labeled cells, which remain unlabeled because the MRI contrast agent is excluded from the nucleus (17). The blastocoel is just beginning to form directly below the labeled cells. The width of the color scale bar represents 125  $\mu\text{m}$ .



a close analog of fluorescent dextran lineage tracers already in use (3), established techniques can be used for its injection into embryonic cells. Unlike the fluorescent probes, which bleach and generate reactive by-products when observed, neither the MRI contrast agent nor the surrounding cytoplasm are perturbed by the process of recording a magnetic resonance image.

To achieve the micrometer-scale resolution necessary to follow developing cell lineages, we used static and gradient magnetic fields several orders of magnitude larger than those used in clinical settings (13). An increase in the resolution from the 1-mm<sup>3</sup> scale of clinical images to the 10- $\mu\text{m}^3$  scale needed here decreases the voxel size by a factor of 10<sup>6</sup>. Because the concentration of water is relatively constant, the signal strength is decreased by the same factor. NMR is an intrinsically low signal-to-noise phenomenon; thus, attempts to measure signals from these small volumes are fraught with difficulties (14). We acquired images at 12- $\mu\text{m}$  resolution using a 7T system with the radio-frequency coil, gradient framework, imaging protocol, and sample preparation optimized for in vivo micrometer-scale imaging (15).

We injected a single blastomere of a 16-cell embryo [blastomere DA (16)] with the Gd-DTPA-dextran tracer and recorded images repeatedly over several days (Fig. 1). The images show the progression from early cleavage and blastula stages (Fig. 1, A to D) through gastrulation (Fig. 1, E to H), neurulation (Fig. 1, I to L), and tail bud stages (Fig. 1, M to P). Arbitrarily oriented serial sections can be extracted from the 3D images (Fig. 2). Progeny of the originally labeled cell appear in the animal hemisphere as a sharply demarcated yellow region occupying the volume expected of eight cells. The several small low-intensity regions in the high-intensity volume (Fig. 2D) are cell nuclei (17). The fluid-filled blastocoel is just beginning to form at this stage and appears at the background intensity level.

Volume representations (Fig. 3, left) and single slices (Fig. 3, right) for an embryo from stages 8 through 21 are shown to illustrate the internal aspects of cell morphogenesis. The clone of labeled cells narrows mediolaterally (converges) and lengthens rostrocaudally (extends) during these stages. At the late blastula stage (Fig. 3A), the labeled clone forms a thick multi-layered patch of contiguous cells. Shortly after the onset of gastrulation (Fig. 3B), the labeled patch has spread, broadened, and elongated, reflecting the movements of epiboly preceding gastrulation. The vegetal edge of the clone of labeled cells has extended around the dorsal lip, highlighting the postinvolution side of the blastopore. After continued convergent extension, the clone reaches the animal pole (Fig. 3C).

The local increase in label intensity along the dorsal midline (Fig. 3C) appears to be the result of a change in cell geometry (columnarization) in the developing neurectoderm, noticeable as a thickening of the labeled neurectoderm. The location of the leading edge of the underlying axial mesoderm as it advances rostrally is correlated with the thickening of the neurectoderm (Fig. 3, B to D). After this geometry change, radial intercalation brings about a radial thinning in the neurectoderm of the labeled clone, which is initiated at the future midbrain-hindbrain border (arrow, Fig. 3E) (18). The radial intercalation in the neurectoderm first spreads caudally (toward the left in Fig. 3E), and later rostrally (Fig. 3F). During the same stages, the underlying chordamesoderm undergoes mediolateral intercalation of labeled and unlabeled cells, as evidenced by the "salt and pepper" pattern of intensities (19). Progressive mediolateral intercalation and rostrocaudal extension continue through to the early neurula with labeled cells along the length of the neural axis (Fig. 3H).

The MRI analysis shows some unexpected correlations, such as those between the thickening of the neurectoderm and the advance of the archenteron. Furthermore, it offers some insights into the choreography of radial intercalation-convergence in the neurectoderm (initiation at the hindbrain-midbrain boundary). Perhaps more surprising is the relative timing of convergence-extension movements in the ectoderm and mesoderm. Because both tissues can undergo convergence movements in cultured explants, many researchers have assumed that these tissues extended the embryonic axis somewhat in concert (20). This assumption would assure that the neurectoderm, and the mesoderm thought to play a role in its induction and patterning, remain coherent during key stages of development. In contrast, the images shown here indicate that the mesoderm undergoes extension movements more rapidly than the surface ectoderm. The archenteron begins its migration behind (caudal) the labeled clone (Fig. 3, B and C); later, it advances past the labeled neurectodermal cells (Fig. 3, E and F); still later, the labeled neurectodermal cells reach as far rostral as the mesodermal cells (Fig. 3H). This mismatch disrupts a strict coherence between layers, which may require some refinements in current proposals of mesoderm-mediated patterning of the ectoderm.

The MRI technique permits structures within the living embryo, usually inaccessible to light microscopy, to be imaged clearly and nondestructively over a period of days. MRI generates a true 3D image from which any arbitrarily oriented 2D slice may be taken that best allows a detailed examina-

tion of the region of interest (Fig. 3). These advantages are not without a cost: When compared to optical images of histological sections, MRI has a smaller signal-to-noise ratio and less resolution. MRI at 50 to 200  $\mu\text{m}$  in-plane resolution has been demonstrated on avian (21) and insect systems (22). Previous studies have indicated the theoretical possibility of MRI in the micrometer resolution range (23). In the images presented here, intrinsic contrast makes internal morphology visible; labeling specific

cells with an MRI contrast agent makes the labeled cells and their descendants distinguishable from surrounding tissue. The ability to follow both labeled cells and surrounding unlabeled tissue has permitted the examination of gastrulation and neurulation in the amphibian embryo, including the relative positions of surface ectodermal cells and deep mesodermal cells over time. Moreover, the changing patterns of MRI label allow us to infer the location and timing of specific types of cellular reorganizations.

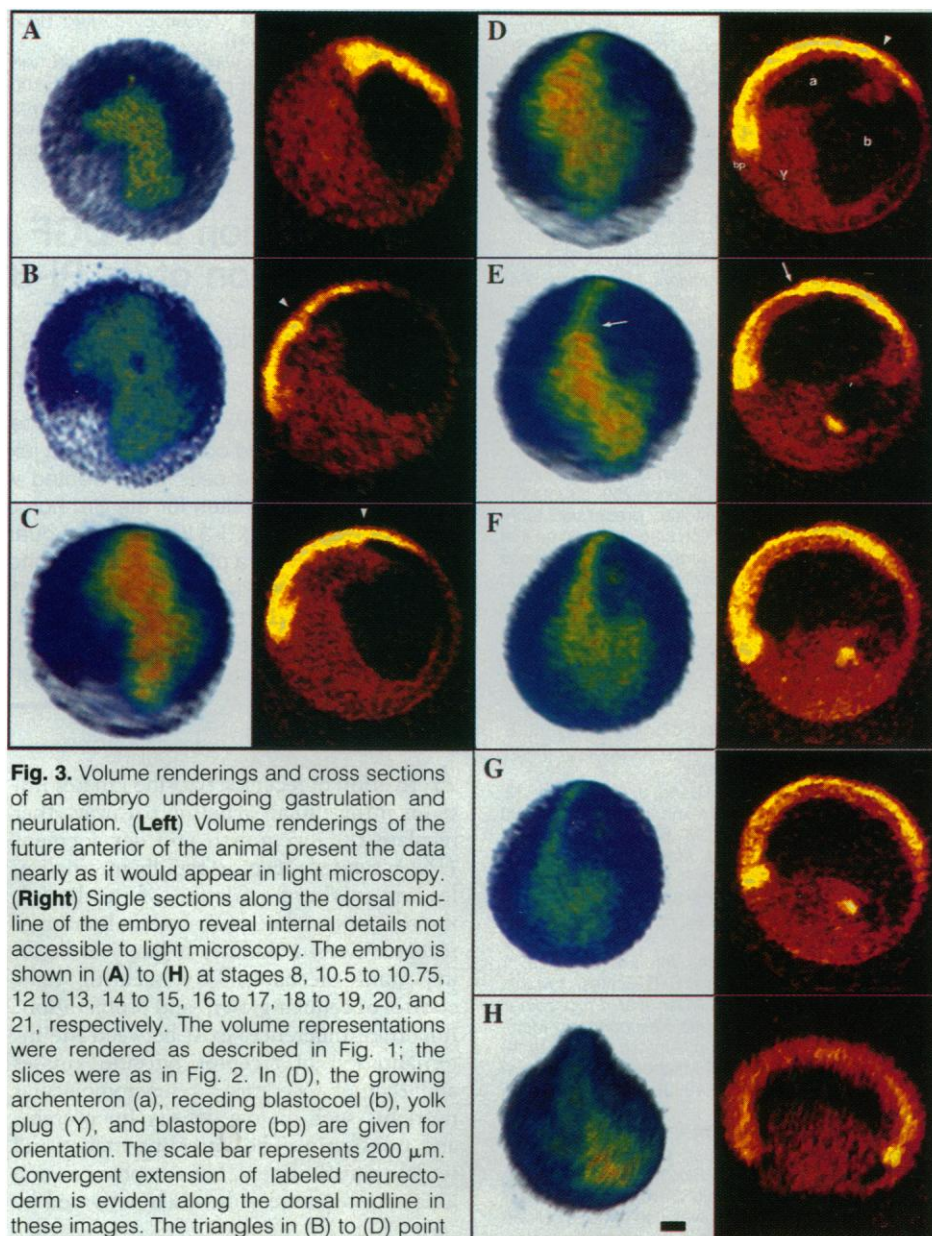


**Fig. 3.** Volume renderings and cross sections of an embryo undergoing gastrulation and neurulation. (Left) Volume renderings of the future anterior of the animal present the data nearly as it would appear in light microscopy. (Right) Single sections along the dorsal midline of the embryo reveal internal details not accessible to light microscopy. The embryo is shown in (A) to (H) at stages 8, 10.5 to 10.75, 12 to 13, 14 to 15, 16 to 17, 18 to 19, 20, and 21, respectively. The volume representations were rendered as described in Fig. 1; the slices were as in Fig. 2. In (D), the growing archenteron (a), receding blastocoel (b), yolk plug (Y), and blastopore (bp) are given for orientation. The scale bar represents 200  $\mu\text{m}$ . Convergent extension of labeled neurectoderm is evident along the dorsal midline in these images. The triangles in (B) to (D) point out the rostral extent of radial thickening of the labeled neurectodermal layer—counterclockwise from each triangle the labeled layer is thicker than it is clockwise. The leading edge of advancing unlabeled axial mesoderm lies immediately below. The arrows in (E) indicate the midbrain-hindbrain junction where extension driven by radial intercalation begins, resulting in thinning of the label. In (E) to (G) there is a separated group of labeled cells in a location consistent with presumptive heart tissue. The DA blastomere gives rise to heart tissue (16) but is thought to do so only at later stages of development. In other sections, a scattered stream of high intensity can be seen connecting the labeled cells in the dorsum with those in the ventrum (25).

## REFERENCES AND NOTES

- J. E. Sulston and H. R. Horvitz, *Dev. Biol.* **56**, 110 (1977); J. E. Kimble and D. Hirsh, *ibid.* **70**, 396 (1979); J. E. Sulston, E. Schierenberg, J. G. White, J. N. Thomas, *ibid.* **100**, 64 (1983); I. S. Greenwald, P. W. Sternberg, H. R. Horvitz, *Cell* **34**, 435 (1983); E. M. Hedgecock, *Trends Neurosci.* **8**, 288 (1985).
- D. A. Weisblat, R. T. Sawyer, G. S. Stent, *Science* **202**, 1295 (1978); H. Balakier and R. A. Pedersen, *Dev. Biol.* **90**, 352 (1982); C. Holt, T. W. Bertsch, H. M. Ellis, W. A. Harris, *Neuron* **1**, 15 (1988).
- D. A. Weisblat, S. L. Zackson, S. S. Blair, J. D. Young, *Science* **209**, 1538 (1980); R. L. Gimlich and J. Braun, *Dev. Biol.* **109**, 509 (1985); M. Bronner-Fraser and S. E. Fraser, *Nature* **335**, 161 (1988); R. Wetts and S. E. Fraser, *Science* **239**, 1142 (1988).
- J. Price, D. Turner, C. Cepko, *Proc. Natl. Acad. Sci. U.S.A.* **84**, 156 (1987); J. R. Sanes, J. L. R. Rubenstein, J.-F. Nicolas, *EMBO J.* **5**, 3133 (1986); D. L. Turner and C. L. Cepko, *Nature* **328**, 131 (1987).
- Zebrafish: C. B. Kimmel and R. M. Warga, *Science* **231**, 365 (1986); sea urchin: R. A. Cameron, S. E. Fraser, R. J. Britten, E. H. Davidson, *Genes Dev.* **1**, 75 (1987).
- P. A. Wilson, G. Oster, R. Keller, *Development* **105**, 155 (1989); R. M. Akers, C. R. Phillips, N. K. Wessels, *Science* **231**, 613 (1986); R. Keller, J. Shih, P. Wilson, *Gastrulation: Movements, Patterns, and Molecules*, R. Keller, W. Clark, and F. Griffen, Eds. (Plenum, New York, 1991).
- M. K. Stehling, R. Turner, P. Mansfield, *Science* **254**, 43 (1991); P. G. Morris, *Nuclear Magnetic Resonance Imaging in Biology & Medicine* (Oxford Univ. Press, New York, 1986); P. Mansfield and P. G. Morris, *NMR Imaging in Biomedicine* (Academic Press, New York, 1982).
- C. T. W. Moonen, P. C. M. van Zijl, J. A. Frank, D. Le Bihan, E. D. Becker, *Science* **250**, 53 (1990).
- We use the steady-state free precession technique with a short repetition time (150 ms) so that the signal is observed preferentially from those spins that return to equilibrium most rapidly (short  $T_1$ ) (7, 23). A short echo time (4.5 ms) is used to minimize  $T_2$  effects.
- D. H. Lee, *J. Can. Assoc. Radiol.* **42**, 6 (1991).
- S. C. Wang *et al.*, *Radiology* **175**, 483 (1990); W. A. Gibby, A. Bogdan, T. W. Oviatt, *Invest. Radiol.* **24**, 302 (1989).
- R. B. Lauffer, *Chem. Rev.* **87**, 901 (1987); G. E. Jackson, S. Wynchank, M. Woudenberg, *Magn. Reson. Med.* **16**, 57 (1990).
- J. B. Aguayo, S. J. Blackband, J. Schoeniger, M. A. Mattingly, M. Hintermann, *Nature* **322**, 190 (1988); G. A. Johnson, M. B. Thompson, S. L. Gewalt, C. E. Hayes, *J. Magn. Reson.* **68**, 129 (1986); R. W. Behling, H. K. Tubbs, M. D. Cockman, L. W. Jelinski, *Nature* **341**, 321 (1989); C. F. Jenner, Y. Xai, C. D. Eccles, P. T. Callaghan, *ibid.* **336**, 399 (1988).
- W. Kuhn, *Angew. Chem. Int. Ed. Engl.* **29**, 1 (1990); P. T. Callaghan and C. D. Eccles, *J. Magn. Reson.* **78**, 1 (1988); P. Glover *et al.*, *Proceedings of the Society of Magnetic Resonance in Medicine, 8th Annual Meeting, Amsterdam, 12 to 18 August 1989* (Society of Magnetic Resonance in Medicine, Berkeley, CA, 1989), p. 285. X. Zhou *et al.*, *ibid.*, p. 286.
- Z. H. Cho *et al.*, *Med. Phys.* **15**, 815 (1988).
- R. Wetts and S. E. Fraser, *Development* **105**, 9 (1989); S. Moody, *Dev. Biol.* **119**, 560 (1987); L. Dale and J. M. W. Slack, *Development* **99**, 527 (1987). Blastomere DA gives rise to head epidermis; retina; lens; portions of the prosencephalon, mesencephalon, and rhombencephalon; and spinal cord.
- The relative size of the MRI label-excluded region is appropriate to the size of nuclei at this stage [W. W. Mathews, *Atlas of Descriptive Embryology* (Macmillan, New York, 1986)], and we have observed that the analogous rhodamine label is excluded from nuclei.
- G. W. Eagleson and W. A. Harris, *J. Neurobiol.* **21**, 427 (1990).
- R. E. Keller, M. Danilichik, R. Gimlich, J. Shih, in *Molecular Biology*, vol. 31 of *New Series*, G. M. Edelman, Ed. (Liss, New York, 1985). The intercalation of deep cells has been observed by Keller and co-workers by grafting tissue with fluorescently labeled cells into unlabeled embryos.
- J. M. W. Slack and D. Tannahill, *Development* **114**, 285 (1992).
- E. L. Efmann, G. A. Johnson, B. R. Smith, G. A. Talbot, G. Cofer, *Teratology* **38**, 59 (1988).
- W. E. Conner, G. A. Johnson, G. P. Cofer, K. Dittrich *et al.*, *Experientia* **44**, 11 (1988).
- C. D. Eccles and P. T. Callaghan, *J. Magn. Reson.* **68**, 393 (1986); C. B. Ahn and Z. H. Cho, *Med. Phys.* **16**, 22 (1989); J. H. Maki, G. A. Johnson, G. P. Cofer, J. R. MacFall, *J. Magn. Reson.* **80**, 482 (1988); P. T. Callaghan, *Principles of Nuclear Magnetic Resonance Microscopy* (Oxford Univ. Press, New York, 1991).
- A single blastomere was pressure-injected with ~20 nl of a solution of Gd-DTPA-dextran (100 mg/ml, 17 kD average molecular mass). Embryos were sealed in a 2.5-mm outer diameter glass NMR tube in 10% Ringer solution and maintained at 17°C. A 1% solution of low-temperature gelling agar in rearing solution was used for later stage embryos to minimize movement. The MRI procedure had no obvious adverse effects on the development of the embryos. A 3D spin echo-pulse sequence with a 150-ms recycle time, 4.5-ms echo time, 10- $\mu$ s dwell time, and 256 by 256 by (32 or 64) data array was used. The time to record a full 3D data set was 90 min. The slice direction data were zero-filled before the 3D Fourier transform to achieve isotropic resolution. Given the strength of the magnetic field gradients used (75 G/cm), this data collection scheme yielded an in-plane pixel resolution of 12  $\mu$ m and a slice thickness of 72 or 36  $\mu$ m.
- R. E. Jacobs and S. E. Fraser, personal observation.
- We thank Z. H. Cho, C. B. Ahn, and S. Juh for assistance in the initial phases of this project; and J. Shih, A. Collazo, and J. Ivins for comments on the manuscript. Supported by National Institutes of Health grant HD 25390, the Baxter Foundation, and a gift from the Monsanto-Searle Company.

27 August 1993; accepted 24 November 1993

## Disruption of PDGF Receptor Trafficking by Mutation of Its PI-3 Kinase Binding Sites

Marguerite Joly, Andrius Kazlauskas, Fredric S. Fay, Silvia Corvera\*

Human platelet-derived growth factor receptors (PDGFRs) expressed in human Hep G2 cells internalized and concentrated in a juxtannuclear region near the Golgi network within 10 minutes after the cells were treated with PDGF. A PDGFR mutant (F5) that lacks high-affinity binding sites for the Src homology 2 domain-containing proteins phosphatidylinositol-3 kinase (PI-3 kinase), Ras guanosine triphosphatase activating protein, phospholipase C- $\gamma$ , and a phosphotyrosine phosphatase (Syp) remained at the cell periphery. Restoration of the PI-3 kinase binding sites on F5 completely restored the ability of the receptor to concentrate intracellularly. A PDGFR mutant lacking only PI-3 kinase binding sites failed to concentrate intracellularly. Thus, PI-3 kinase binding sites appear both necessary and sufficient for the normal endocytic trafficking of the activated PDGFR.

Activation of receptor tyrosine kinases initiates intracellular signaling pathways that regulate cellular growth and development (1). Activated receptors rapidly internalize, leading to the degradation of the ligand, the receptor, or both (2). Internalization of receptor tyrosine kinases is likely to be an important mechanism for securing tight control of cellular growth and proliferation. Important differences exist between the internalization of receptor tyrosine kinases and that of receptors for macromolecular nutrients such as low density lipoproteins and transferrin. The latter internalize and recycle constitutively, but receptor tyrosine kinases internalize only when activated by

ligand (2). Ligand binding induces autophosphorylation on tyrosines of the receptor cytoplasmic domain and its association with signaling proteins that contain Src homology 2 domains. These include phospholipase C- $\gamma$  (PLC- $\gamma$ ), the guanosine triphosphatase activating protein for Ras (GAP), the 65-kD phosphotyrosine phosphatase (Syp), nonreceptor tyrosine kinases (3), and PI-3 kinase (4). This enzyme catalyzes the phosphorylation of phosphatidylinositol (PIs), PIns(4)P, and PIns(4,5)P<sub>2</sub> at the 3' position of the inositol ring, but the biological functions of these lipids are not known.

We tested the hypothesis that the trafficking of receptor tyrosine kinases is driven by the regulatory proteins that are recruited to the autophosphorylated cytoplasmic domain. The activated PDGFR binds to a large number of regulatory proteins (5) and is rapidly internalized and degraded (6). The role of regulatory proteins in the internalization and trafficking of the human  $\beta$ -PDGFR was analyzed in cells expressing

M. Joly and S. Corvera, Program in Molecular Medicine and Department of Cell Biology, University of Massachusetts Medical School, 373 Plantation Street, Worcester, MA 01605.

A. Kazlauskas, National Jewish Hospital for Immunology and Respiratory Medicine, Denver, CO 80206.  
F. S. Fay, Program in Molecular Medicine and Biomedical Imaging Group, University of Massachusetts Medical School, Worcester, MA 01655.

\*To whom correspondence should be addressed.